AFRL-RY-WP-TR-2011-1121

THEORY AND DEVICE MODELING FOR NANO-STRUCTURED TRANSISTOR CHANNELS

Isaiah P. Steinke and P. Paul Ruden

University of Minnesota

JUNE 2011
Final Report

AIR FORCE RESEARCH LABORATORY
SENSORS DIRECTORATE
WRIGHT-PATTERSON AIR FORCE BASE, OH 45433-7320
AIR FORCE MATERIEL COMMAND
UNITED STATES AIR FORCE

NOTICE AND SIGNATURE PAGE

Using Government drawings, specifications, or other data included in this document for any purpose other than Government procurement does not in any way obligate the U.S. Government. The fact that the Government formulated or supplied the drawings, specifications, or other data does not license the holder or any other person or corporation; or convey any rights or permission to manufacture, use, or sell any patented invention that may relate to them.

This report was cleared for public release by the USAF 88th Air Base Wing (88 ABW) Public Affairs Office (PAO) and is available to the general public, including foreign nationals. Copies may be obtained from the Defense Technical Information Center (DTIC) (http://www.dtic.mil).

AFRL-RY-WP-TR-2011-1121 HAS BEEN REVIEWED AND IS APPROVED FOR PUBLICATION IN ACCORDANCE WITH ASSIGNED DISTRIBUTION STATEMENT.

*//Signature//

MARK PACER, Project Engineer
Metamaterials Branch
Aerospace Components Division

//Signature//

JACQUELINE TOUSSAINT, Chief
Metamaterials Branch
Aerospace Components Division

//Signature//

JEFF HUGHES, Chief
Aerospace Components Division
Sensors Directorate

This report is published in the interest of scientific and technical information exchange, and its publication does not constitute the Government's approval or disapproval of its ideas or findings.

*Disseminated copies will show "//Signature//" stamped or typed above the signature blocks.

REPORT DOCUMENTATION PAGE

Form Approved
OMB No. 0704-0188

1. REPORT DATE *(DD-MM-YY)*	2. REPORT TYPE	3. DATES COVERED *(From - To)*
June 2011	Final	30 June 2008 – 30 May 2011

4. TITLE AND SUBTITLE
THEORY AND DEVICE MODELING FOR NANO-STRUCTURED TRANSISTOR CHANNELS

5a. CONTRACT NUMBER
FA8650-08-C-1444

5b. GRANT NUMBER

5c. PROGRAM ELEMENT NUMBER
62204F

6. AUTHOR(S)
Isaiah P. Steinke and P. Paul Ruden

5d. PROJECT NUMBER
2002

5e. TASK NUMBER
11

5f. WORK UNIT NUMBER
2002110A

7. PERFORMING ORGANIZATION NAME(S) AND ADDRESS(ES)
University of Minnesota
Department of Electrical Engineering
200 Union Street
Minneapolis, MN 55455

8. PERFORMING ORGANIZATION REPORT NUMBER

9. SPONSORING/MONITORING AGENCY NAME(S) AND ADDRESS(ES)
Air Force Research Laboratory
Sensors Directorate
Wright-Patterson Air Force Base, OH 45433-7320
Air Force Materiel Command
United States Air Force

10. SPONSORING/MONITORING AGENCY ACRONYM(S)
AFRL/RYDM

11. SPONSORING/MONITORING AGENCY REPORT NUMBER(S)
AFRL-RY-WP-TR-2011-1121

12. DISTRIBUTION/AVAILABILITY STATEMENT
Approved for public release; distribution unlimited.

13. SUPPLEMENTARY NOTES
PAO Case Number: 88 ABW-11-3365; Clearance Date: 13 Jun 2011. This report contains color.

14. ABSTRACT
We have developed two models to describe the behavior of field-effect transistors with nano-structured channels. The primary factor that limits the performance of the transistor is the presence of grain boundaries. In our macroscopic model, we have explicitly modified the field-effect mobility to include terms that are dependent upon both the local carrier concentration and longitudinal field. In our mesoscopic model, we more closely look at the role of the individual grains by incorporating ideas from percolation theory. In this model, the carrier statistics are connected to the site and bond occupation probabilities in the site-bond percolation problem in order to determine the threshold voltage.

15. SUBJECT TERMS
nano-structured transistor, mesoscopic, zinc oxide, ZnO, field-effect transistor, device model

16. SECURITY CLASSIFICATION OF:			17. LIMITATION OF ABSTRACT:	18. NUMBER OF PAGES	19a. NAME OF RESPONSIBLE PERSON (Monitor)
a. REPORT	b. ABSTRACT	c. THIS PAGE			Mark Pacer
Unclassified	Unclassified	Unclassified	SAR	32	19b. TELEPHONE NUMBER *(Include Area Code)* N/A

TABLE OF CONTENTS

LIST OF FIGURES

1.0 SUMMARY

The Theory and Device Modeling for Nano-Structured Transistor Channels program began on 9 June 2008 and the technical effort concluded by 6 May 2011. It was executed by the Department of Electrical and Computer Engineering at the University of Minnesota with Prof. P.Paul Ruden serving as PI. Dr. Isaiah P. Steinke was the key technical contributor to the program.

The principal effort of the program focused on theoretical work that raises significantly the level of understanding of transport phenomena in nano-structured materials. Of particular interest were materials that are under active exploration for the fabrication of field-effect transistors. Although the specific calculations focused on zinc oxide FETs, the models developed and explored are quite general and will be a foundation for further work that may address other materials.

2.0 INTRODUCTION

The work for this program has been focused on developing models for nanostructured field-effect transistors in order to better understand how grain boundaries impact field effect transistor performance. This was motivated by the results published by Bayraktaroglu[1] for zinc oxide (ZnO) thin film transistors (TFTs) that contain nanocrystalline grains on the order of ~20nm. The authors of ref. 1 present results that show a gate bias dependent field-effect mobility that reaches ~100$cm^2V^{-1}s^{-1}$, which suggests that the mobility is dependent upon the carrier concentration in the channel. The grain boundaries in the channel are thought to be the primary limitation for the performance of these devices since grain boundaries represent potential barriers that impede the motion of free carriers in the channel. Trapped charge at the grain boundaries causes the formation of energy barriers between the grains. These energetic barriers between the grains may be lowered by the presence of additional free carriers or by the application of an electric field, thus enhancing the grain-to-grain transport.

We have formulated two different models to account for the role of the grain boundaries in the performance of these transistors. The first model developed was a "macroscopic" model, where we modified the expression for the field-effect mobility of the electrons in the transistor channel to be dependent upon both the local carrier concentration and the longitudinal electric field. This model is referred to as macroscopic since it inherently averages over multiple grains. The second model we developed was intended to examine more closely the role of individual grains in the transistor channel. We have called this model the "mesoscopic" model, and it incorporates ideas from percolation theory. In this model, the relative populations of electrons in each grain influence the transport of carriers across the grain boundary by changing the magnitude of the potential barriers between grains. Since percolation concepts are useful in describing phase transitions, this model describes the transistor when the channel goes from nonconducting to conducting at the threshold voltage.

3.0 METHODS, ASSUMPTIONS, AND PROCEDURES

3.1 Macroscopic Model Theory

We now describe the basic theory for our macroscopic model and summarize some of the main results. In our macroscopic model, we assume that the transport in the channel is dominated by the drift current, and that the diffusion contribution to the current is negligible. It is also assumed that the gradual channel approximation holds, such that we can write the local sheet carrier concentration, $n(x)$, as a function of position along the channel as:

$$n(x) = -\frac{C}{e}\left(V_{ch}(x) - V_{GS}\right), \tag{1}$$

where C is the gate capacitance per unit area, e is the elementary charge, $V_{ch}(x)$ is the potential at a point x along the channel, and V_{GS} is the applied gate bias. The longitudinal field $F(x)$ is related to the local carrier concentration by:

$$F = -\frac{\partial V_{ch}}{\partial x} = \frac{e}{C}\frac{dn}{dx}. \tag{2}$$

Since the longitudinal field is directly proportional to the gradient of the carrier concentration, we can write a general expression for the density- and field-dependent mobility, μ, solely in terms of n and its gradient as:

$$\mu = \mu_0 + an^p + b\left(\frac{dn}{dx}\right)^q, \tag{3}$$

where μ_0, a, b, p, and q are all model parameters. The expression in equation 3 is our modified mobility that accounts for the presence of free carriers and the application of a longitudinal field that act to decrease the energy barriers at the grain boundaries. Hereafter we will refer to the mobility terms an^p and $b(dn/dx)^q$ in our discussion of this model as the carrier density dependent and longitudinal field dependent mobility terms, respectively. Consistent with the standard model for field effect transistors, we assume that the current in the channel is dominated by the drift current, and we write the current density, j, as:

$$j = -e\mu nF = -\frac{e^2}{C}\mu n\left(\frac{dn}{dx}\right). \tag{4}$$

If the carrier density profile is known, we can use equation 4 to solve for the current density. However, in general the carrier density profile is unknown and we solve for $n(x)$ under dc bias conditions, by noting that the current density does not change with position along the channel (i.e. $dj/dx = 0$). We can then transform equation 4 into a nonlinear second order differential equation in n:

$$\frac{dj}{dx} = 0 = \frac{d}{dx}\left[\mu n \frac{dn}{dx}\right]. \tag{5}$$

Equation 5 is subject to the boundary conditions at the source and drain ends of the channel (using equation 1):

$$n(0) = n_s = \frac{C}{e}(V_{GS} - V_T) \text{ and} \tag{6a}$$

$$n(L) = n_d = \frac{C}{e}(V_{GS} - V_{DS} - V_T) = n_s - \frac{C}{e}V_{DS}, \tag{6b}$$

where n_s and n_d are the carrier concentrations at the source and drain ends of the channel, respectively, L is the channel length, V_{DS} is the applied drain bias, and V_T is the threshold voltage. We can find the drain bias at which the current saturates, $V_{DS,sat}$, by noting that the concentration at the drain end must always be non-negative:

$$V_{DS,sat} = \frac{e}{C} n_s = V_{GS} - V_T, \tag{7}$$

which is the same as in the standard field effect transistor model.

Equation 5 for $n(x)$ is analytically solvable in the case where the mobility is constant or in the case where the carrier density dependent mobility term is included.[2] However, if we include the longitudinal field dependent mobility term, equation 5 becomes difficult to solve analytically and we instead solve it by numerical integration. With the boundary conditions given by equations 6a and 6b, we have a two-point boundary value problem that we solve via a relaxation method. The constant mobility solution given in ref. 2 is the initial seed for the carrier density profile at a fixed V_{GS} and V_{DS}. We discussed the basic solution methodology in detail in references 3 and 4.

3.2 Mesoscopic Model Theory

We now turn to the details of our mesoscopic model. As stated earlier, percolation can be used to describe sharp phase transitions, and our mesoscopic model is used to describe the transition of the nanocrystalline transistor channel from nonconducting to conducting. The basics of percolation have been discussed in an earlier status report,[5] and we will not repeat the details of percolation theory here. Our mesoscopic model uses a site-bond percolation problem on a 2D triangular lattice as a basis. We illustrated the basic ideas of the simpler site percolation problem on a 2D triangular lattice in a previous status report,[6] where we saw the appearance of a lattice-spanning cluster formed near the percolation threshold. In other status reports, we described two important percolation quantities, the percolation probability,[7] P, and the conductance,[8] G, of the lattice-spanning cluster.

We represent the nanocrystalline grains in the channel as the individual sites of the lattice located at the vertices of each triangle in our site-bond percolation problem. The relative number of free

carriers within the grain is described by the site occupation probability and is related to the local voltage drop across the gate insulator within the framework of the gradual channel approximation. In short, the grains are considered conducting or nonconducting due to the presence or absence of carriers in that part of the channel. The energetic barriers due to the presence of trapped charge at the grain boundaries are represented as bonds on the lattice. We relate the bond occupation probability to the magnitude of the energetic barriers between grains. As in our macroscopic model, these energy barriers are influenced by the carrier concentration and by an applied longitudinal field.

In a field effect transistor, the total number of carriers in the channel may be modulated by the gate bias, V_G. We can write the relationship of V_G to the total sheet density of carriers, n_{total}, via the formula:

$$n_{total} = \frac{CV_G}{e} + n_B, \tag{8}$$

where the extra carrier density term n_B is included to represent a background of charge under zero applied gate bias. This background of carriers can either be thermally excited carriers in the conduction band or pre-existing trapped carriers and can be used to account for a non-zero threshold voltage. It is assumed that the carriers in the channel either populate conduction band states in the grains, n, or trap states within the grain boundaries, n_T. The total carrier sheet density in the channel is then related to these two quantities by:

$$\frac{CV_G}{e} + n_B = n_T + n = N_T f_T + N_C f_C, \tag{9}$$

where N_T is the (average) total number of trap states per unit area at the grain boundaries, N_C is the two-dimensional effective conduction band density of states, and f_C and f_T are the occupation probabilities given by:

$$f_C = \exp\left[\left(E_F - E_C\right)/k_B T\right] \text{ and} \tag{10}$$

$$f_T = \frac{1}{1+\exp\left[\left(E_T - E_F\right)/k_B T\right]}, \tag{11}$$

where E_F is the (quasi) Fermi energy, E_C is the conduction band energy, E_T is the energy level of the trap states in the grain boundaries, k_B is Boltzmann's constant, and T is the absolute temperature. Since we are mainly interested in the behavior of the transistor near the threshold voltage, we have assumed that the occupation of states within the grain is non-degenerate in equation 10. We rewrite f_T in equation 11 using equation 10 as:

$$f_T = \frac{1}{1+\frac{N_C}{n}\exp\left[\left(E_T - E_C\right)/k_B T\right]}. \tag{12}$$

We can then substitute equations 10 and 12 into equation 9 and solve for n in terms of the gate bias and grain boundary trap parameters, ($E_C - E_T$) and N_T. Once we have solved for n, we can calculate n_T and thus define the probability that a site is occupied as:

$$p_s \equiv \frac{n}{n + n_T}, \tag{13}$$

which is just the fraction of carriers available for conduction for a given gate bias.

This derivation was also detailed in an earlier status report,[9] where we plotted the variation of n and p_s as a function of V_G in which the model parameters $E_C - E_T$ and N_T were also varied. For shallow trap energy levels, we found that there was enough thermal energy at low gate voltages such that not all trap states are filled and a significant number of carriers are free for conduction. However, for relatively deep trap levels at low gate voltage, a vast majority of the carriers induced by the gate voltage get trapped at the grain boundaries. Essentially no free carriers are available until a large enough gate bias is applied and all of the available trap states are filled. We also found that there is a distinct voltage at which n and p_s start to have a value greater than zero when the trap state is deep enough (usually ~$7k_BT$). When investigating the effect of N_T by fixing the trap level at midgap, we found that for a relatively low number of total traps ($N_T = 10^{10}$ cm^{-2}), almost any applied gate voltage is enough to produce free carriers regardless of the location of the trap energy level.

We derived an expression for the energy barriers due to the grain boundaries by assuming that a sheet of negative charge exists at the grain boundary due to trapped carriers.[10] We considered the simplest case: one grain boundary with two grains, one on either side of the grain boundary. In a one-dimensional model, the presence of trapped charge at the grain boundary creates a depletion region of width W on either side of the grain boundary. It was assumed that the grains are semi-infinite (i.e. not fully depleted). Later, we will find that this assumption is valid for the range of gate biases we are interested in near the threshold voltage, but the derivation with a finite grain size can also be done.

To find an expression for the energy barriers at the grain boundary, we performed the straightforward one-dimensional electrostatics analysis based on the Poisson equation:

$$\frac{d^2V}{dx^2} = -\frac{\rho(x)}{\varepsilon_S \varepsilon_0}, \tag{14}$$

where ε_S is the relative dielectric constant for the semiconductor ($\varepsilon_S = 7.8$ for ZnO[11]), and $\rho(x) = +en^{(3)}$ for $-W < x < W$. The volume density associated with the sheet density n is given by $n^{(3)} = n/\chi$, where χ is the thickness of the inversion layer in the channel (taken to be ~ 5 nm). Integration of equation 14 yields the solution for the electric field, $F(x)$, for each grain on either side of the grain boundary separately. Due to the presence of the sheet charge at $x = 0$, the solutions for the electric field at 0^- and 0^+ differ by $|en_T/\varepsilon_S\varepsilon_0|$. Under equilibrium conditions, $F(-W) = F(W) = 0$ and we find that $2n^{(3)}W = n_T$, as expected for charge neutrality.

Upon integration of the expressions for electric field, we obtained the profile for the electric potential, V, as a function of x. We then found the expression for the barrier height, V_b, by noting that $V_b = V(0) - V(-W)$ or $V(0) - V(W)$ in equilibrium:

$$|V_b| = \frac{en_T^2 \chi}{8\varepsilon_S \varepsilon_0 n}, \tag{15}$$

The behavior of the grain boundary barrier height with gate bias was shown by varying both $E_C - E_T$ and N_T with no background of carriers.[10] In general, the barrier height is zero when the gate bias is zero and then increases to a maximum. When there are a significant number of free carriers available, the barrier height then decreases back to a small value. An increase in either $E_C - E_T$ or N_T will increase the maximum value that the barrier height attains.

Having derived an expression for the grain boundary barrier height, we now discuss the bond occupation probability. We think of the bond occupation probability as the possibility that a bond on the lattice is conducting or nonconducting. We assume that electrons in the channel can move between the grains if they have enough energy to surmount the energetic barrier present at the grain boundary (i.e. through thermal excitation) and we define p_b as:

$$p_b \equiv \exp\left(-eV_b / k_B T\right). \tag{16}$$

We note that the bond occupation probability is dependent upon both the free carrier and trapped carrier concentrations via V_b, which is in turn dependent upon the gate bias V_G.

4.0 RESULTS AND DISCUSSION

4.1 Results using the Macroscopic Model

We first summarize our macroscopic model by looking at the general effects of including the additional mobility terms in equation 3 by looking at the addition of each term separately.[12] For the results presented here, we have set our model parameters to be: $\mu_0 = 20\text{cm}^2/\text{V}\cdot\text{s}$, $a = 5.5\times10^{-12}\text{cm}^4\text{V}^{-1}\text{s}^{-1}$, $b = 10^{-32}\text{cm}^8\text{V}^{-1}\text{s}^{-1}$, $a = 1$, and $b = 2$. Other physical device parameters, as well as gate and drain biases used to generate the output and transfer characteristics, are taken or estimated from the paper by Bayraktaroglu.[1]

Figure 1 shows the carrier profile along the channel at the onset of saturation for an applied gate bias of 8V with the addition of either the carrier density or longitudinal field dependent mobility terms. As a baseline comparison, we have included the analytical constant mobility solution also. In Figure 1, we see that the addition of the carrier density and longitudinal field dependent mobility terms have opposite effects when compared to the constant mobility carrier profile. With the addition of the carrier density dependent mobility term, the carrier density is increased along the channel, whereas the carrier density is lowered when the longitudinal field dependent mobility term is added. However, this lowering of the carrier density along the channel increases the carrier density gradient.

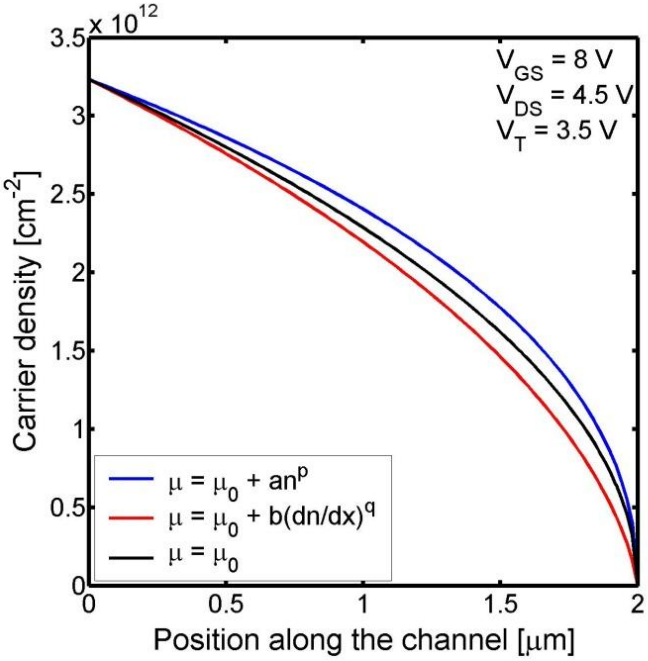

Figure 1. Carrier density as a function of channel position at the onset of saturation individually illustrating the effects of the carrier density and longitudinal field dependent mobility terms for V_{GS} = 8V.

In Figure 2 and Figure 3, we have plotted the longitudinal electric field and the contribution to mobility of each additional mobility term as a function of the position along the channel, respectively. Here again, we see that the mobility terms have opposite effects. As expected from Figure 1, we see that the longitudinal electric field is larger near the source end and throughout much of the channel when the field dependent mobility term is used since the gradient of the carrier density is larger. When including the carrier density dependent term, we see in Figure 1 that the carrier density increases all along the channel and the slope is decreased except near the drain end. Thus, we see in Figure 2 that the longitudinal electric field is lowered except near the drain end.

As can be expected from the carrier density profiles in Figure 1, the carrier density is at a maximum at the source end and the gradient of the carrier density is largest at the drain end of the channel. Thus, we expect the contribution to mobility to be highest at the source for the carrier density dependent term and highest near the drain for the field dependent term, as we see in Figure 3.

A comparison of the output and transfer characteristics from the inclusion of the carrier density and longitudinal field dependent mobility terms is shown in Figure 4 and Figure 5, respectively.

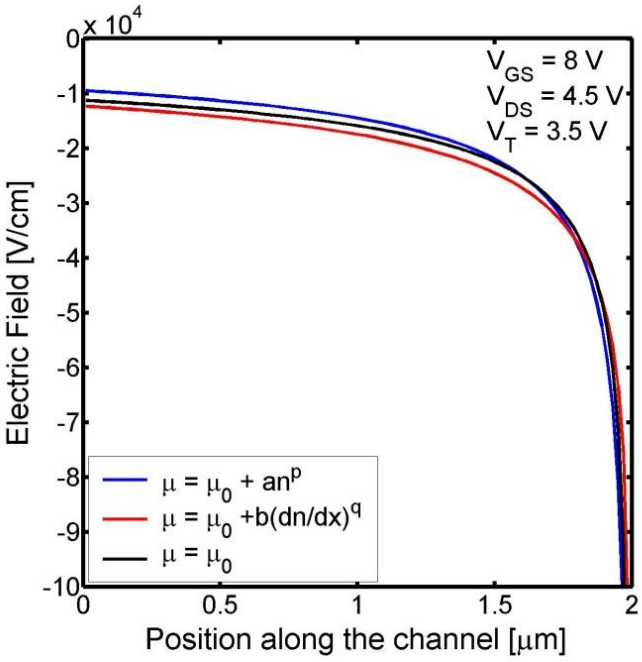

Figure 2. Plot of the longitudinal electric field along the channel for the data in Figure 1.

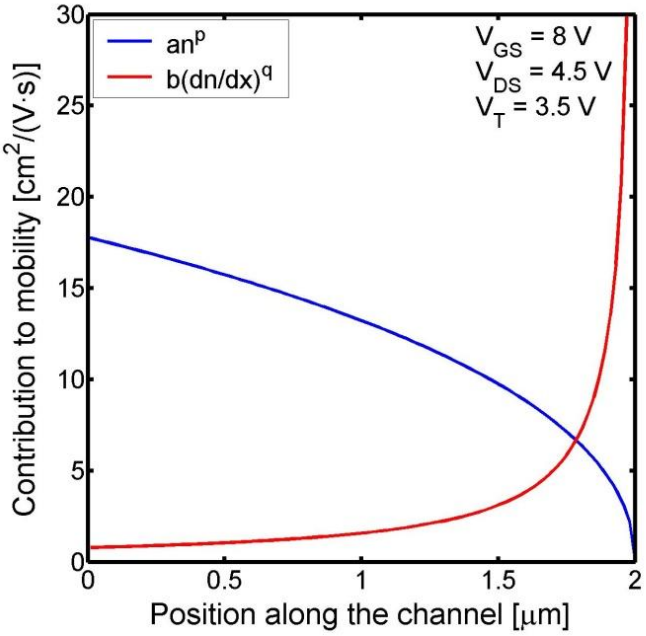

Figure 3. Contribution to mobility for the carrier density and longitudinal field dependent mobility terms along the channel length for the data shown in Figure 1.

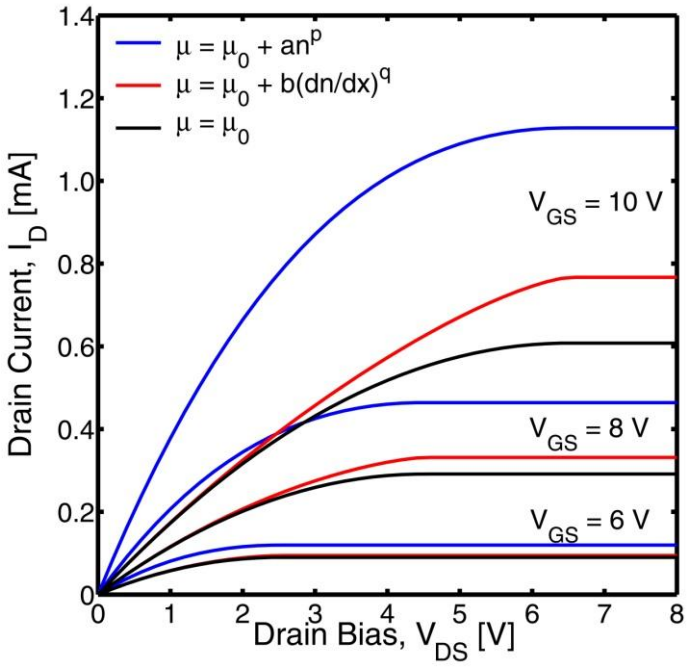

Figure 4. I_D-V_{DS} characteristics illustrating the effect of the carrier density and longitudinal field dependent mobility terms.

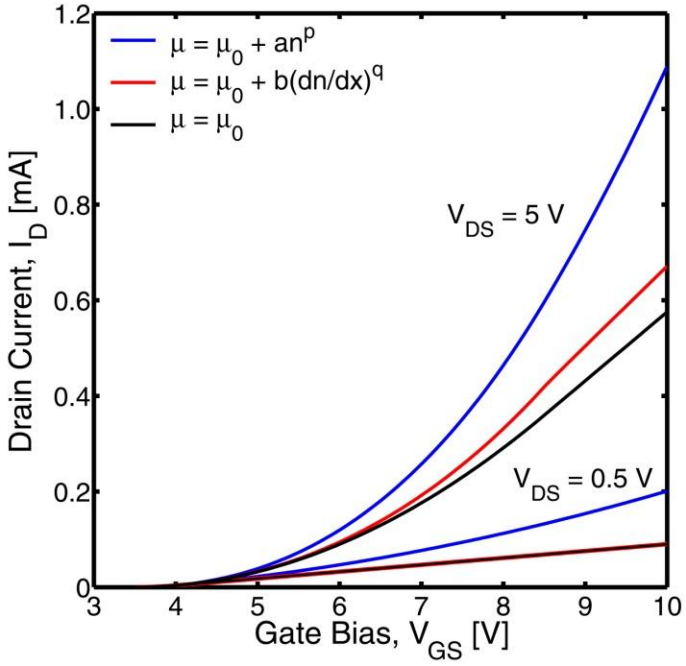

Figure 5. I_D-V_{GS} characteristics showing the effect of the carrier density and longitudinal field dependent mobility terms.

For the model parameters used, we find that the addition of the carrier density dependent mobility term yields the largest current for a given gate and drain bias. From equation 4, we see that the combination of carrier density dependent mobility term as well as the increase in the carrier density along the channel offset the lowering of the carrier density gradient for a net increase in current. We also find that at low drain bias (and hence low longitudinal electric field) that the field dependent mobility term does not contribute much to the drain current, as seen in Figure 5 for V_{DS} = 0.5V. The triode regime of the output characteristic in Figure 4 is also different, as the field dependent mobility term appears to "flatten" this portion of the characteristic.

As one might expect, when including both extra mobility terms at the same time, the results tend to offset.[13] As discussed in ref. 13, the carrier density and longitudinal field as a function of position more closely follow the constant mobility solution, with the some deviation at the source and drain ends of the channel due to the presence of these extra mobility terms. However, the additional mobility terms have a similar contribution to mobility to the results shown in Figure 3, and the drain current in the output and transfer characteristics was greatly increased.

The magnitude of the applied drain bias has a large influence on the contribution of longitudinal field dependent mobility term.[13] For the results presented here, we have biased the transistor at the onset of saturation. In ref. 13, we found that even a 33% reduction in drain bias from $V_{DS,sat}$ is enough to reduce the contribution to mobility of the longitudinal field dependent term such that the contribution to mobility from the carrier density dependent mobility term is greater throughout the entire channel. As stated earlier, our results in Figure 5 showed that for a small

drain bias of 0.5V, the addition of the longitudinal field dependent mobility term is not enough to significantly alter the magnitude of the drain current from the constant mobility case.

To conclude our discussion of the macroscopic model, we show how well the model can fit the output characteristics presented by Bayraktaroglu below saturation.[1] We have extracted the values for μ_0, a, and V_T by fitting the channel conductance using the output characteristics in the linear regime ($V_{DS} < 0.5$V) with $p = 1$. Using the necessary experimental device parameters from ref. 1, we find that $\mu_0 = 160\text{cm}^2\text{V}^{-1}\text{s}^{-1}$, $a = 10^{-11}\text{cm}^4\text{V}^{-1}\text{s}^{-1}$, and $V_T = 4$V. In Figure 6, we have plotted the experimental data as open circles along with two curves using the model: the dashed line is with the addition of the carrier density dependent mobility only, and the solid line additionally includes the longitudinal field dependent mobility term with $b = 7\times10^{-32}\text{cm}^8\text{V}^{-1}\text{s}^{-1}$ and $q = 2$. We find that the fit to the experimental output characteristics is good for low values of V_{DS} when just the carrier density dependent mobility term is included, but does not adequately fit at higher values of V_{DS} and V_{GS}. With the addition of the longitudinal field dependent mobility term, we can improve the fit to the experimental data over the entire range of V_{DS} at large values of V_{GS}.

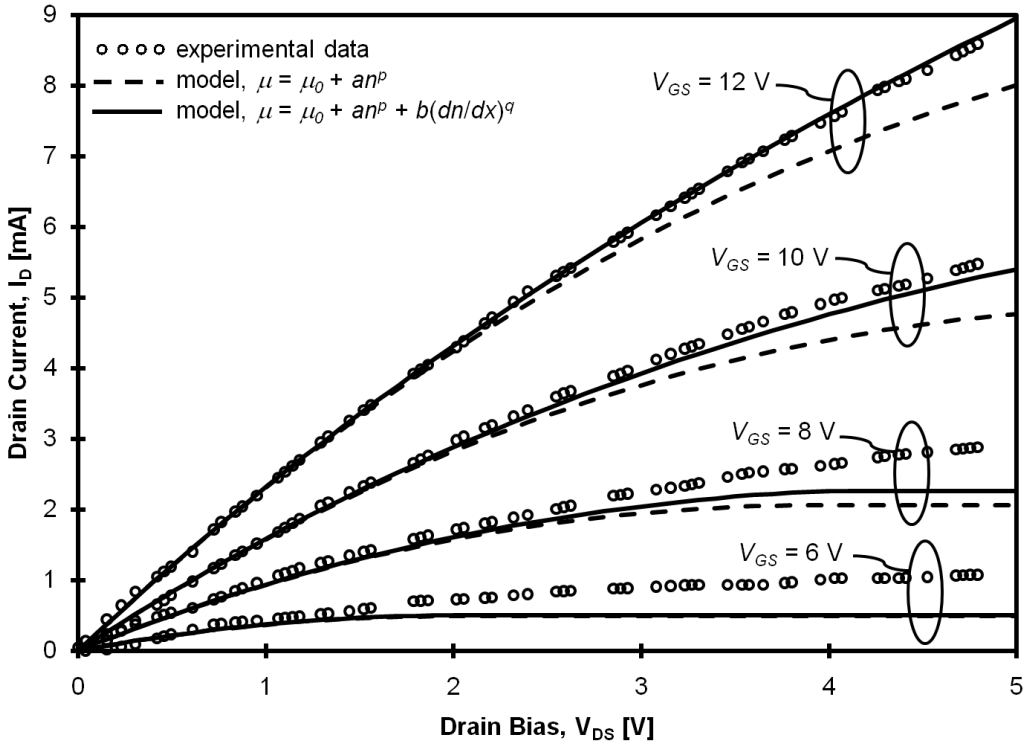

Figure 6. Macroscopic model fit to the experimental data presented in ref. 1. See text for model parameters used.

4.2 Results using the Mesoscopic Model

We now summarize the results of our mesoscopic model. Previously, we investigated[14] the variation of both the site and bond occupation probabilities as a function of V_G for $N_T = 10^{12}$ cm^{-2} and $E_C - E_T = 6k_BT$ and $8k_BT$. It was found that the bond occupation probability has a different dependence on V_G than the site occupation probability. With no background of carriers present, the bond occupation probability is quite high at zero gate bias and then quickly decreases to almost zero. Only once a significant density of free carriers is available again to lower the barrier height will the bond occupation probability then increase. When a shallower trap level is used, the bond occupation probability does not go as low since there is a greater possibility of free carriers available.

Now that we see that both the site and bond occupation probabilities are determined by the applied gate bias, we connect these quantities to the site-bond percolation problem to determine the threshold voltage.[15] The sudden appearance of the lattice-spanning cluster in the site-bond problem represents a change in the lattice from a nonconducting to a conducting state. With the use of Monte Carlo simulations, we have determined this threshold for the site-bond percolation problem in $p_b - p_s$ space for a 50×50 triangular lattice. As discussed earlier, both the site and bond occupation probabilities may be determined for a given gate bias and model parameters. The intersection of these mesoscopic model curves as determined by the carrier statistics with the site-bond percolation threshold curves represents the gate bias necessary to reach the threshold voltage.

In the last status report,[16] we determined the threshold voltage as a function of one of the model parameters, $E_C - E_T$. It was found that the magnitude of the threshold voltage reached a limit when $E_C - E_T$ was increased to ~$7k_BT$, after which it remained constant. This result was true even when the total density of traps and the temperature are varied. For the same trap energy, increasing the total density of traps or decreasing the temperature will increase the magnitude of the threshold voltage.

We now look at the variation of the threshold voltage with two other model parameters, N_T and T. In Figure 7, we have plotted the site-bond thresholds for the square and triangular lattices along with the mesoscopic model curves in which we have varied N_T and fixed $E_C - E_T = 6k_BT$ and $T = 300$ K. In Figure 8, we have also plotted these thresholds and curves when T is varied and $E_C - E_T = 5k_BT$ and $N_T = 10^{12}$ cm^{-2}. We find that when T is increased that we appear to reach a limiting value of (p_s, p_b) whereas we do not when N_T is varied.

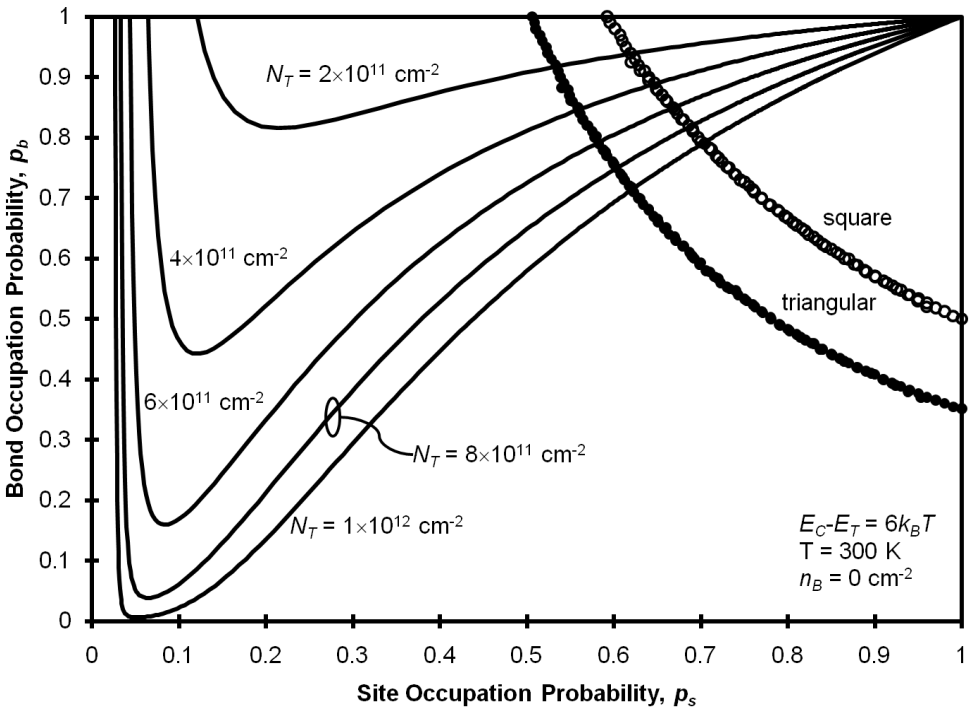

Figure 7. Plot of the mesoscopic model curves and site-bond threshold data used to determine V_T. The various mesoscopic model curves are for different values of N_T.

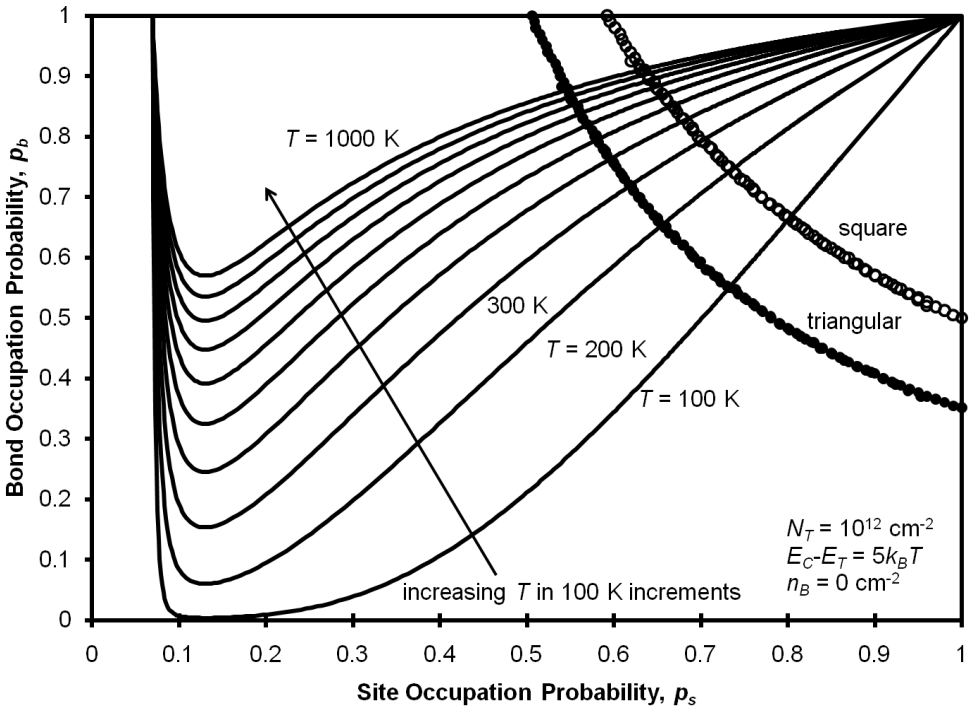

Figure 8. Plot of the mesoscopic model curves and site-bond threshold data used to determine V_T. The various mesoscopic model curves are for different values of T.

To explore this further, we have extracted the threshold voltages as a function of N_T for various $E_C - E_T$ in Figure 9 and various T in Figure 10. In both figures, we see that dependence of V_T on N_T appears to be linear over the range of N_T considered. However, we do see that both $E_C - E_T$ and T appear to limit the magnitude of the threshold voltage (e.g. the very small differences in the $E_C - E_T = 6k_BT$ and $9k_BT$ data points in Figure 9).

Similarly, we explore the variation of the threshold voltage with T for various values of N_T and $E_C - E_T$ in Figures 11 and 12, respectively. In both of these figures we find that the threshold voltage appears to saturate as the temperature is increased. In Figure 11, we see that the spacing of data points at a fixed temperature is incrementally the same with respect to N_T, as was concluded before where V_T varied approximately linearly with N_T. We also find in Figure 12 that once $E_C - E_T$ has been increased sufficiently high; the magnitude of the threshold voltage does not increase appreciably.

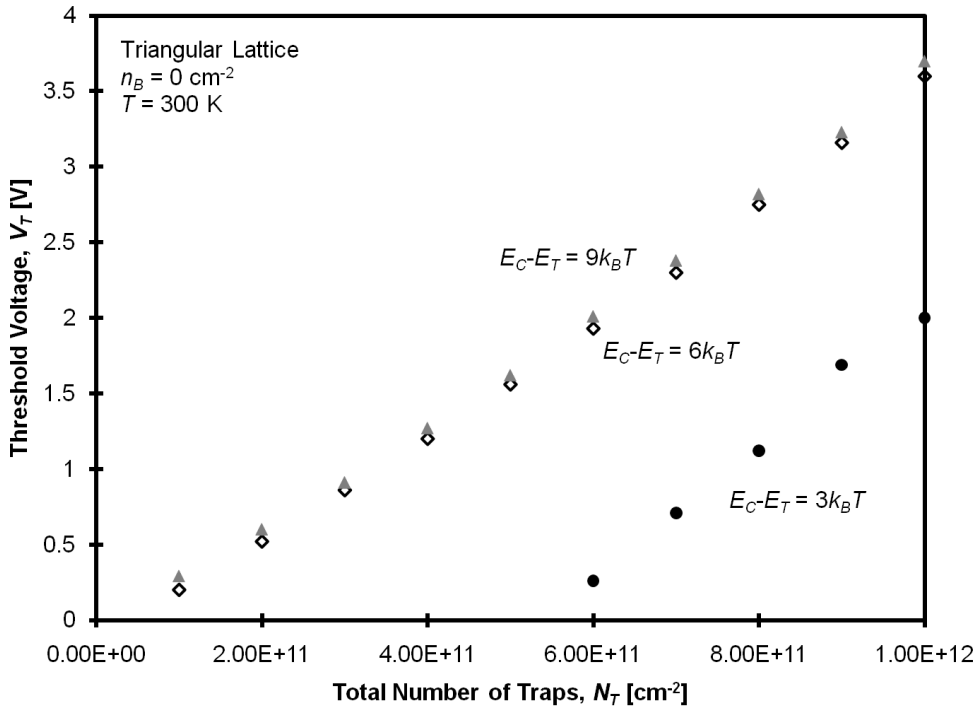

Figure 9. Variation of threshold voltage as a function of N_T for various trap depths below the conduction band.

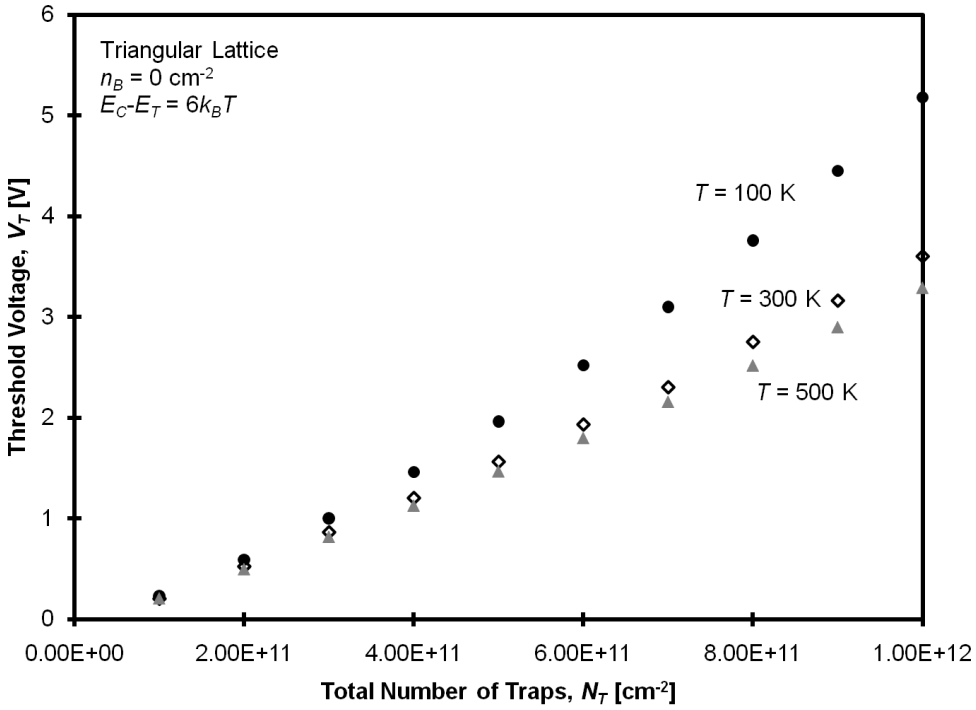

Figure 10. Variation of threshold voltage as a function of N_T for various temperatures.

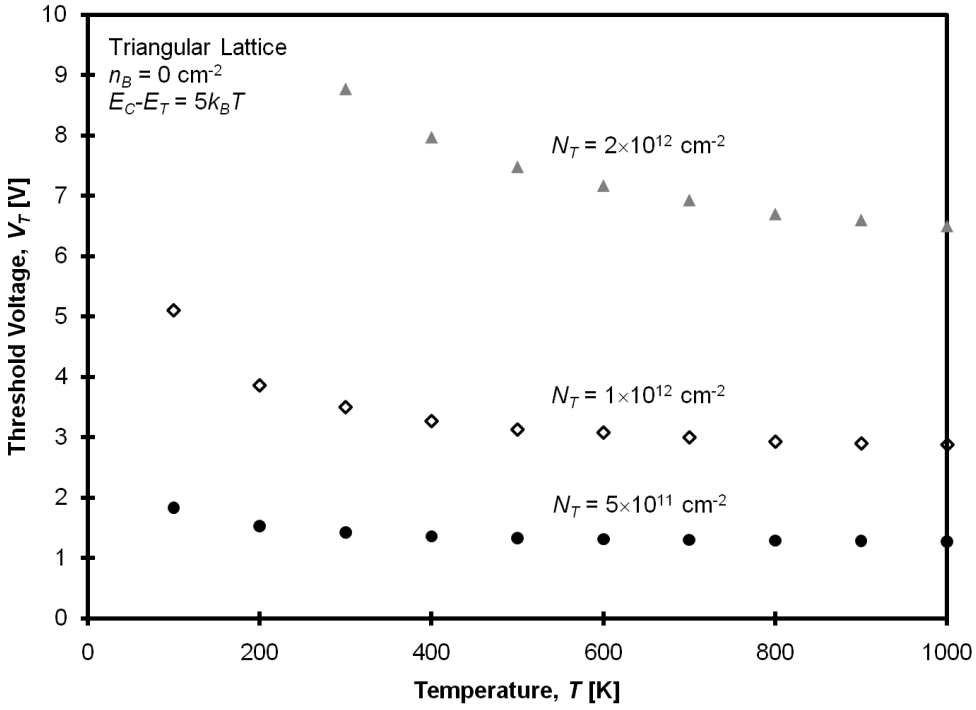

Figure 11. Variation of threshold voltage as a function of temperature for different values of N_T.

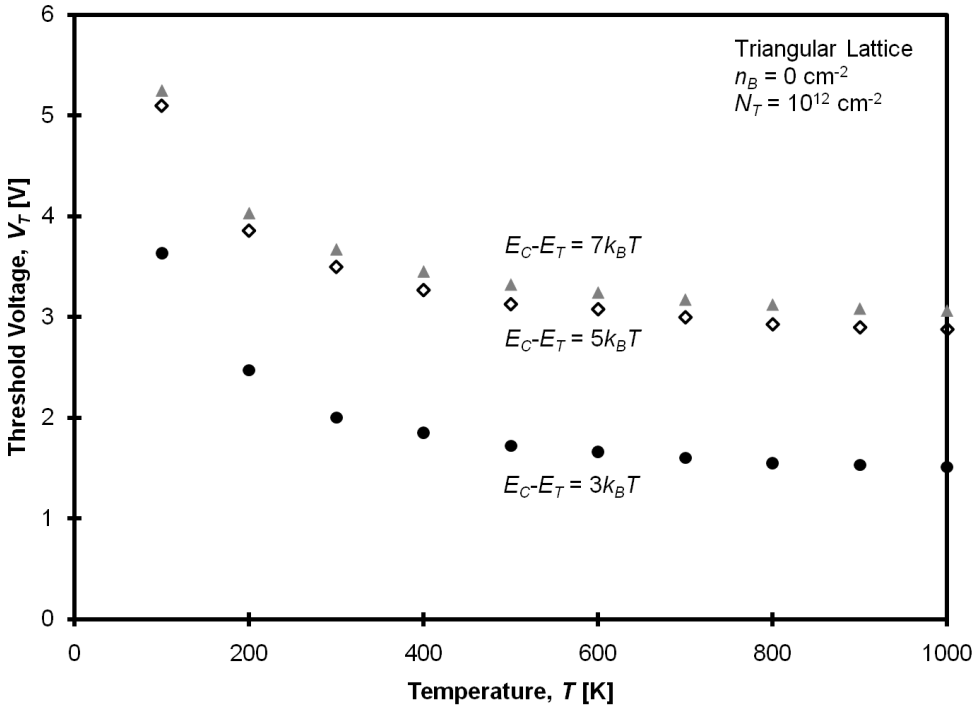

Figure 12. Variation of threshold voltage as a function of temperature for $E_C - E_T$.

5.0 CONCLUSIONS

We have described two models to explain the behavior of a nano-structured field-effect transistor. The channels in this type of device contain multiple grain boundaries that are the primary limitation in their performance. These grain boundaries introduce energetic barriers that electrons in the channel must overcome in order to move from one grain to another. The magnitude of this energetic barrier may be altered by the free carrier concentrations in the two grains separated by the grain boundary, or by the application of a longitudinal electric field.

In our macroscopic model, we have explicitly modified the mobility to include dependencies upon the local sheet carrier concentration and the longitudinal electric field in order to account for the aforementioned grain boundary energy barrier lowering effects. With the use of the gradual channel approximation, we have written the longitudinal field in terms of the gradient of the carrier density. This yielded an expression for the current density that can be written solely in terms of the local carrier concentration. We found the values for the carrier density along the channel by using a relaxation method to solve the nonlinear second-order differential equation that results when the longitudinal field dependent mobility term is included.

We first explored the effects of including each of the extra mobility terms separately. In general, we found that the presence of the carrier density dependent mobility term increases the magnitude of the carrier concentration throughout the channel. However, the presence of the longitudinal field dependent mobility term did the opposite, lowering the carrier density throughout the channel, thereby increasing the carrier concentration gradient. We also found opposite effects when we looked at the contribution to mobility for each of these mobility terms. The carrier density dependent mobility term made its greatest contribution to the mobility at the source where the carrier density was largest, whereas the longitudinal field dependent mobility term made its greatest contribution at the drain end, where the carrier density gradient was largest. Lastly, we found that the addition of either term increases the overall magnitude of the current density when compared with the constant mobility case.

As one would expect, when both mobility terms were used at the same time, the result was that they offset each other, as seen in the carrier density and field profiles. However, there is still a large increase in the overall current density. We also found that the longitudinal field dependent mobility term was influenced by the magnitude of the applied drain bias. When we modestly decreased the magnitude of the applied drain bias, we found a lower contribution to the mobility from the longitudinal field dependent mobility term. For very small drain biases (< 0.5V), the additional contribution to the current density due to the longitudinal field dependent mobility term was negligible.

We demonstrated the use of our macroscopic model by fitting the output characteristics to the nano-structured ZnO transistors grown by Bayraktaroglu . Using the channel conductance data in the linear region of the output characteristics, we extracted the macroscopic model parameters for V_T, μ_0, and a. The addition of only the carrier density dependent mobility term showed a good fit to the experimental data at relatively low drain bias. We were able to achieve a much better fit to the output characteristics throughout the triode regime by adding the longitudinal field dependent mobility term.

The shortcoming of our macroscopic model is that it inherently averages over multiple grains in the channel. In order to incorporate the effects of the individual grains in the nano-structured channel, we developed a mesoscopic model. This model uses percolation theory to account for the statistical variation in grains. Specifically, we used a site-bond percolation problem on a 2D triangular lattice. The sites on this lattice were represented by the grains in our transistor channel and were occupied if there was a significant fraction of free carriers available. The bonds on the lattice were represented by the energy barriers between neighboring grains and were occupied if this energy barrier was small enough. Both of these quantities were controlled by the applied gate bias, which determined the population of free carrier states in the grain and trap states at the grain boundary.

One of the main features of percolation is that an abrupt phase transition occurs when the critical percolation threshold has been reached. In our nano-structured transistor, this transition represents the transistor channel 'turning on' when we have reached the threshold voltage. Using multiple Monte Carlo simulations for the site-bond percolation problem, we determined the site-bond percolation threshold in $p_b - p_s$ space. We then combined this threshold with the site and bond occupation probabilities determined using the carrier statistics in our mesoscopic model. When these two curves intersect, we have reached the gate voltage at which percolation occurs and have determined the threshold voltage for the transistor.

We have explored the variation in the threshold voltage with the adjustable parameters in our mesoscopic model: $E_C - E_T$, N_T, and T. We found that when we decreased the energy of the trap state below the conduction band edge, the threshold voltage increased until we reached ~$7k_BT$, after which the threshold voltage remained constant. We found a similar limitation when increasing the temperature except that increasing the temperature decreases the magnitude of the threshold voltage. When the total concentration of traps at the grain boundary was increased, we found that the magnitude of the threshold voltage increased linearly with no limiting value.

Both models developed are quite general inasmuch as they can be applied to field effect transistors with a wide range of nanostructured channel materials. Both also can be extended to overcome their present limitations. Specifically, the macroscopic model calls for an extension into the saturation regime such as to model the finite output conductance in saturation displayed by the current experimental output characteristics. The mesoscopic model can be readily extended beyond the linear regime by including the local variation of the occupation probabilities for sites and bonds into the Monte Carlo simulations that yield the channel conductance. In a simple approximation, this local variation could be determined within the gradual channel approximation as obtained from the macroscopic model. Overall, the models developed here represent a very good starting point for further theoretical explorations of field effect transistors with nanostructured channel materials.

6.0 REFERENCES

[1] B. Bayraktaroglu, K. Leedy, and R. Neidhard, "Microwave ZnO Thin-Film Transistors", *IEEE Electron Dev. Lett.* **29**, 1024 (2008); doi: 10.1109/LED.2008.2001635.

[2] Steinke, I. P. and Ruden, P. Paul, *Theory and Device Modeling for Nano-Structured Transistor Channels*, Bimonthly Status Report for Dec 2008 – Jan 2009, University of Minnesota, Minneapolis, MN.

[3] Steinke, I. P. and Ruden, P. Paul, *Theory and Device Modeling for Nano-Structured Transistor Channels*, Bimonthly Status Report for Feb 2009 – Mar 2009, University of Minnesota, Minneapolis, MN.

[4] Steinke, I. P. and Ruden, P. Paul, *Theory and Device Modeling for Nano-Structured Transistor Channels*, Bimonthly Status Report for Apr 2009 – May 2009, University of Minnesota, Minneapolis, MN.

[5] Steinke, I. P. and Ruden, P. Paul, *Theory and Device Modeling for Nano-Structured Transistor Channels*, Bimonthly Status Report for Jun 2009 – Jul 2009, University of Minnesota, Minneapolis, MN.

[6] Steinke, I. P. and Ruden, P. Paul, *Theory and Device Modeling for Nano-Structured Transistor Channels*, Bimonthly Status Report for Dec 2009 – Jan 2010, University of Minnesota, Minneapolis, MN.

[7] Steinke, I. P. and Ruden, P. Paul, *Theory and Device Modeling for Nano-Structured Transistor Channels*, Bimonthly Status Report for Aug 2010 – Sep 2010, University of Minnesota, Minneapolis, MN.

[8] Steinke, I. P. and Ruden, P. Paul, *Theory and Device Modeling for Nano-Structured Transistor Channels*, Bimonthly Status Report for Oct 2010 – Nov 2010, University of Minnesota, Minneapolis, MN.

[9] Steinke, I. P. and Ruden, P. Paul, *Theory and Device Modeling for Nano-Structured Transistor Channels*, Bimonthly Status Report for Feb 2010 – Mar 2010, University of Minnesota, Minneapolis, MN.

[10] Steinke, I. P. and Ruden, P. Paul, *Theory and Device Modeling for Nano-Structured Transistor Channels*, Bimonthly Status Report for Apr 2010 – May 2010, University of Minnesota, Minneapolis, MN.

[11] K. Ellmer, "Resistivity of Polycrystalline Zinc Oxide Films: Current Status and Physical Limit", J. Phys. D **34**, 3097 (2001); doi: 10.1088/0022-3727/34/21/301.

[12] Steinke, I. P. and Ruden, P. Paul, *Theory and Device Modeling for Nano-Structured Transistor Channels*, Bimonthly Status Report for Aug 2009 – Sep 2009, University of Minnesota, Minneapolis, MN.

[13] Steinke, I. P. and Ruden, P. Paul, *Theory and Device Modeling for Nano-Structured Transistor Channels*, Bimonthly Status Report for Oct 2009 – Nov 2009, University of Minnesota, Minneapolis, MN.

[14] Steinke, I. P. and Ruden, P. Paul, *Theory and Device Modeling for Nano-Structured Transistor Channels*, Bimonthly Status Report for Jun 2010 – Jul 2010, University of Minnesota, Minneapolis, MN.

[15] Steinke, I. P. and Ruden, P. Paul, *Theory and Device Modeling for Nano-Structured Transistor Channels*, Bimonthly Status Report for Dec 2010 – Jan 2011, University of Minnesota, Minneapolis, MN.

[16] Steinke, I. P. and Ruden, P. Paul, *Theory and Device Modeling for Nano-Structured Transistor Channels*, Bimonthly Status Report for Feb 2011 – Mar 2011, University of Minnesota, Minneapolis, MN.

LIST OF SYMBOLS, ABBREVIATIONS, AND ACRONYMS

a	coefficient for the carrier density mobility term (macroscopic model)
b	coefficient for the longitudinal field mobility term (macroscopic model)
C	gate capacitance
e	elementary charge
E_C	conduction band energy
E_F	Fermi energy
E_T	trap level energy
f_c	occupation probability for free carriers
f_T	occupation probability for trapped carriers
$F(x)$	longitudinal field along the channel
G	conductance of the lattice-spanning cluster
$j(x)$	current density
k_B	Boltzmann's constant
L	channel length
n_B	background sheet charge concentration
N_C	two-dimension effective conduction band density of states
$n^{(3)}$	depleted charge density in the grain
n_d	sheet carrier concentration at the drain end of the channel
n_s	sheet carrier concentration at the source end of the channel
N_T	total density of traps at the grain boundary
n_T	trapped sheet carrier concentration
n_{total}	total sheet carrier concentration

$n(x)$	sheet carrier concentration or free carrier density
P	percolation probability
p	exponent for the carrier density mobility term (macroscopic model)
p_b	bond occupation probability
p_s	site occupation probability
q	exponent for the longitudinal field mobility term (macroscopic model)
T	absolute temperature
TFT	thin film transistor
V	electric potential
V_b	grain boundary energy barrier height
$V_{ch}(x)$	potential at point x along the channel
V_{DS}	applied drain bias
$V_{DS,sat}$	saturation drain bias
V_{GS}, V_G	applied gate bias
V_T	threshold voltage
W	gate width
ZnO	zinc oxide
χ	effective channel thickness
ε_0	dielectric constant in vacuum
ε_S	relative dielectric constant for the semiconductor
μ	field-effect mobility
μ_0	constant mobility term (macroscopic model)
$\rho(x)$	charge density